Self-sieving DNA over superhydrophobic surfaces: A Raman spectroscopy study

Received: 22 November 2021 | Revised: 22 March 2022 | Accepted: 19 April 2022

DOI: 10.1002/jrs.6368

RESEARCH ARTICLE

Journal of RAMAN SPECTROSCOPY WILEY

Self-sieving DNA over superhydrophobic surfaces: A Raman spectroscopy study

Monica Marini[1] | **Bruno Torre**[1] | **Marco Allione**[1] | **Tania Limongi**[1] | **Francesca Legittimo**[1] | **Andrea Giugni**[2] | **Carlo Ricciardi**[1] | **Candido Fabrizio Pirri**[1,3] | **Enzo di Fabrizio**[1]

[1]Dipartimento di Scienza Applicata e Tecnologia (DISAT), Politecnico di Torino, Torino, Italy

[2]Physics Department, Università Degli Studi di Milano, Milan, Italy

[3]Istituto Italiano di Tecnologia (IIT), Torino, Italy

Correspondence
Monica Marini, Dipartimento di Scienza Applicata e Tecnologia (DISAT), Politecnico di Torino, Torino, Italy.
Email: monica.marini@polito.it

Abstract

The Raman spectra of DNA fibers were studied before and after suspension over superhydrophobic surface (SHS). At the end of the dehydration process of a droplet of nucleic acids solution over SHS, two structural areas appear: (i) a thicker droplet residual spot and (ii) a thinner free-standing, self-oriented DNA extended fibers region. For specimens deposited on reference samples (CaF_2 slides), buffer contribution overrides the total Raman spectrum, while for free-standing λDNA, biological signature comes out readily with no interference. Our spectroscopy results confirm that a mechanical sieving effect occurs spontaneously during λDNA suspension process over superhydrophobic devices. Tailored designed devices and sample preparation separate small non-interacted molecules from the bundles and remove, concentrating, the non-suspended material in a defined area of the SHS. At the end of the process, helices retain only the ions that effectively have interacted with the DNA strand in solution, while all the other compounds were sieved away from the areas of interest. The self-sieving effect herein shown will provide a step forward for biomaterials studies as it allows the characterization of dilutions otherwise not detectable. The samples, autonomously purified, retain the effective interaction with environmental stresses free from any other misleading contribution allowing for characterization in optimal condition.

KEYWORDS

free-standing DNA, micro-Raman, self-sieving, superhydrophobic devices

1 | INTRODUCTION

DNA is widely used for its biological meaning and as a constructive material in bionanotechnology, for sensing and detection purposes.[1–3] Many of these applications rely on the use of purified DNA strands of various lengths, ranging from a few bases to several kilobases. Pure long DNA are commonly obtained by the removal of all the other solution constituents with processes of increasing complexity[4] on the bases of the length (e.g., with columns and precipitation[5–7]). DNA purification is of fundamental importance in several molecular

biology applications. In the purification process, critical aspects are the protection from enzymatic degradation and shearing caused by mechanical stress.[8] Although DNA chemical synthesis is also commercially available, it faces several limitations. The available DNA lengths are limited to a maximum of 200 nucleotides,[9] and, depending on the scale, purification, size and modification required, the synthesis can be expensive, with low yields or too complex to be accomplished.[10] In this context, obtaining long DNA molecules free from shearing and contributions from buffers or other biomolecules can still be a hurdle.

A recent approach exploits the use of micro-fabricated superhydrophobic surfaces (SHS) to obtain free-standing and self-organized biological material[11] including DNA filaments.[12–14] The biomaterial is dispersed in a physiological environment and is suspended over the SHS in a single-step process. The droplet reduces its volume due to water evaporation at controlled temperature and humidity conditions and moves from one pillar to the following. In this movement, the drop drags the biomolecules in solution, originating an ordered suspended grid over the SHS. With this method, biomolecules such as DNA, DNA/protein complexes and cell membranes with their embedded proteins have been successfully imaged by Transmission Electron Microscopy (TEM) and High-Resolution TEM (HRTEM).[15,16] Characteristic features and diffraction spacing of an A-DNA helix were found in good agreement with those obtained by conventional X-Ray diffraction.[17,18] With free-standing DNA, for the first time, base pairs and the phosphate backbone were directly measured. Suspended DNA was also studied with vibrometry[16] to achieve mechanical information on the fibers. Direct imaging and vibrational information can be combined with data about the state of the biomaterials analyzed in terms of structural overview and interaction with the environment. To this end, Raman spectroscopy is a powerful non-destructive tool[19] used on the suspended materials to get valued insights of details related to biomolecular conformations and to materials not prone to crystallization.[20]

Here, we report the study of suspended genetic material on SHS in presence of different physiologically compatible buffers by Raman spectroscopy to demonstrate the sieving effect on double strand nucleic acids, at increasing environment complexity, performed by the SHS. Autonomous sieving and suspension of biosamples applied to Raman spectroscopy offer clear advantages if compared to more conventional approaches such as crystallography. The sample preparation follows a straightforward procedure, while the number of the molecules investigated simultaneously dramatically reduces, allowing for the detection and study of localized variation regarding pristine molecules. Recently, micro-Raman spectroscopy and SHS were proposed to study the DNA conformations and evaluate single or double-strand DNA.[21,22] Also, access to pure materials results in major importance for Raman analysis allowing the rapid acquisition of the contextual signatures of intrinsic biomolecules for the refined comparison analysis of unknown samples. Applying SHS approach, we obtained long DNA fibers free from any additional environmental contributions, standing isolated from each other, stable in air or vacuum being not covered or affected by the presence of any liquid solution.

2 | RESULTS AND DISCUSSION

Four physiologically compatible buffers with different characteristics (see Section 5) were used in this work to suspend and dehydrate the droplet. The solutions containing mono or divalent cations are commonly used in cell and molecular biology experiments to provide physiological-compatible environment (buffers 1–3; see Section 5) or to facilitate nucleic acids adsorption in imaging procedures[23] (buffers 3 and 4; see Section 5). Depositing a droplet containing nucleic acids over a SHS, we obtained oriented DNA bundles in all the cases.[12,13,15,24] The evaporation of the buffer solution and the SHS geometry allows concentrating the material in a delimited and precise device area. In the evaporation process, the droplet is deposited at the center of the device and reduces its volume and shrinks towards its center, moving preferentially from one pillar to the neighbor. DNA strands linked to the tops of the pillars are stretched across the gap between adjacent pillars and cover the pillar–pillar distance of approximately 12 μm. At the end of the droplet dehydration process, it is possible to distinguish two main areas on the same device. As reported in the Scanning Electron Microscopy (SEM) micrograph of Figure 1a, the presence of non-interacted material is confined to a limited part of the SHS, the droplet residual, over approximately a diameter of 400 μm. The area covered by the residual is 1 order of magnitude smaller than the droplet initial footprint, confirming the device concentration capability.[25] All around the residual fibers are observed, straight and clean from salt crystals or other impurity residuals (Figure 1b,c). The cross-section diameter of the bundles ranges between 200 nm towards the droplet residual to diminish down to 6 nm in the outer area where the droplet evaporation starts. The extension of the area covered by the suspended DNA helices is approximately 600 μm, in good agreement with previously published data.[17,22]

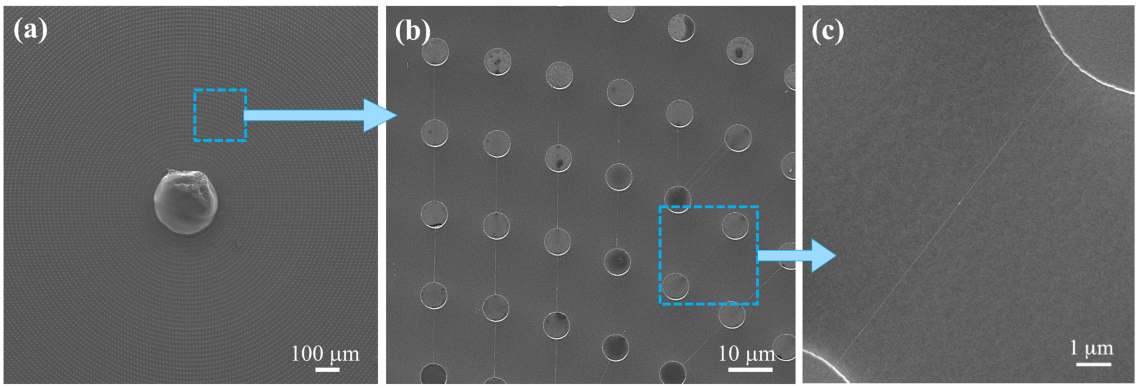

FIGURE 1 SEM images of free-standing DNA filaments on superhydrophobic surfaces. (a) The droplet residual, confined in a precise part of the device and surrounded by suspended DNA filament of different diameters. (b) An area with DNA bundles of a diameter ranging between 100 and 20 nm. (c) A zoomed view of a bundle with a diameter of approximately 35 nm [Colour figure can be viewed at wileyonlinelibrary.com]

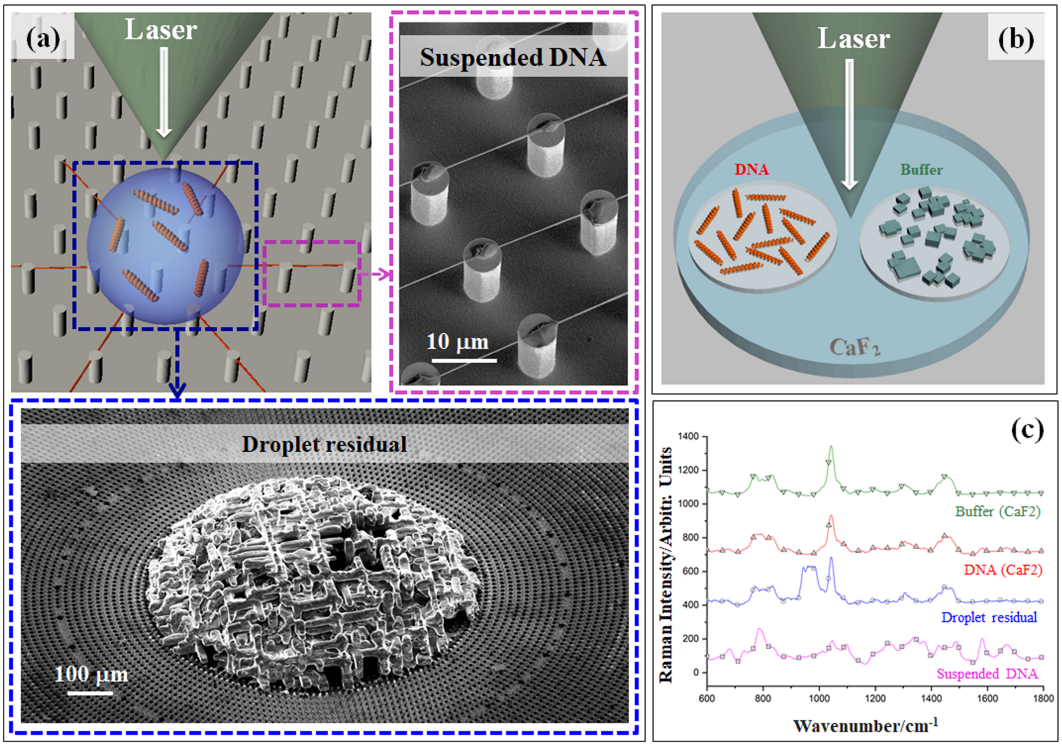

FIGURE 2 (a) General Scheme of the evaporation process; suspended samples; (b) samples deposited on CaF_2 windows used in this work and (c) related spectra of samples in a $NiCl_2$ + HEPES working buffer [Colour figure can be viewed at wileyonlinelibrary.com]

2.1 | Superhydrophobic device sieving effects and buffer interference

We use Raman spectroscopy to study the droplet dehydration results and compare them with data collected using support substrates characterized by a very low fluorescence signal, such as CaF_2 windows. In Figure 2 are reported sketches of the areas related to the Raman measurements over SHS and CaF_2 windows.

We acquired two sets of data on each different substrate:

1. Silicon SHS devices (Figure 2a):

a. droplet residual
b. suspended dsDNA filament (Figures 1b and 2a).

2. CaF_2 windows (Figure 2b):

a. buffer only
b. DNA in the buffer.

The data collected on DNA filaments and the droplet residual were compared with those acquired on DNA samples and buffer deposited over a commercial CaF_2 window (Figure 2c). A full set of each of the four different samples was prepared and measured for all the buffers used. All the measurements were performed after the droplet dehydration at a relative humidity lower than 75%.

2.2 | SELF-PURIFICATION OF SUSPENDED DNA FIBERS

The nucleic acid spectra showed the characteristic fingerprints of the nucleic acids molecules as well as several conformation-sensitive vibrations related to the DNA phosphate group, the deoxyribonucleic sugar and the bases[26–28] (Figure 3).

In our experimental conditions, buffers composed of monovalent (Na^+) or divalent (Mg^{2+}) cations and Tris-HCl-buffering agent (Figure 3a,b) showed a Tris-HCl Raman contribution with characteristic main peaks[29] at around 760, 1064 and 1467 cm^{-1} that practically dominated all the spectra. An aliquot of λDNA diluted in Tris-buffered solution and drop-casted on a CaF_2 conventional window was also analyzed by Raman spectroscopy. The spectra acquired (Figure 3) showed characteristic DNA peaks aside strong contribution of the Tris-cation, suggesting that residuals of buffer were retained by the sample. The three main bands of the buffer overlapped with DNA bands and strongly interfered with the data interpretation. The interference occurs in several areas of the nucleic acid spectra: (i) the range 700–800 cm^{-1}, related to the DNA phosphate backbone, the O-P-O DNA marker and the cytosine (C) breathing mode[22,30,31]; (ii) at ~1061 cm^{-1} corresponding to the vibration of the covalent bond between the deoxyribose sugar and the phosphate group of the DNA backbone[32] and (iii) at 1463 cm^{-1}, related to the 5′CH_2 scissor mode and the guanine (dG) base.[31,33–35] These bands are too close to the bands related to Tris-buffer to clearly distinguish between the DNA and Tris-cation contributions. The relative ratios between the main peaks in the buffer and DNA on CaF_2 spectra are comparable and due to buffer presence rather than DNA presence. Also, the subtraction of the buffer signal to the DNA spectra will lead to incorrect or misleading band assignments due to the overlap of the spectra.

The spectra acquired on the droplet residual (Figure 3, blue line) showed wavenumbers and intensities comparable to those observed for the buffer solution.

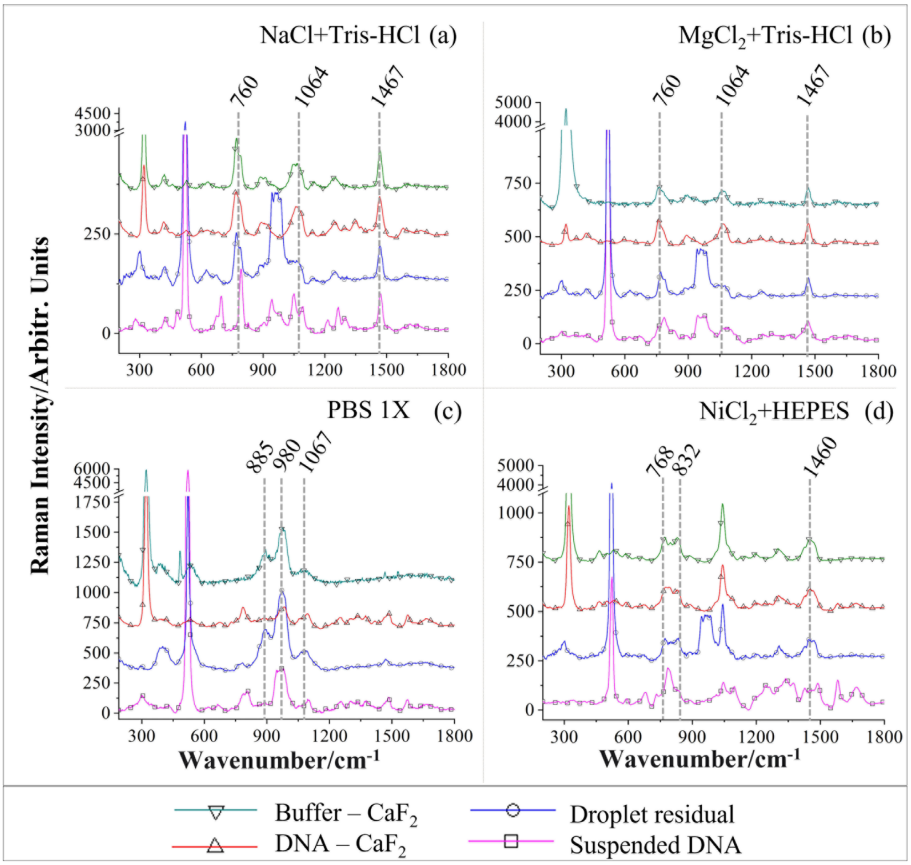

FIGURE 3 Spectra of working buffer, DNA on standard CaF2 substrate (not suspended), droplet residual and DNA suspended on SHS for (a) NaCl+TrisHCl, (b) $MgCl_2$ + TrisHCl, (c) PBS 1× and (d) $NiCl_2$ + HEPES. Dotted lines highlight the prominent buffer bands contributions [Colour figure can be viewed at wileyonlinelibrary.com]

The additional features in the region 900–1000 cm^{-1} are related to the secondary peak of the silicon device.

The analysis of the suspended DNA fingerprint spectral region revealed spectra free from any Tris-cation contribution. Features of dsDNA were observed in the spectral range 600–1800 cm^{-1}.[36,37] In the interval (iv) 640–730 cm^{-1}, there are details on the conformational properties (A/B conformation) of the double helix; between (v) 750 and 900 cm^{-1} are enclosed information related to the phosphate backbone, while the region (vi) 1000–1700 cm^{-1} is sensitive the sugar/base conformation. In the case of suspended material, peaks centered at 789 and 1468 cm^{-1} are assigned to phosphate backbone and 5′CH_2 scissor mode, respectively, rather than to the Tris-cation due to the absence of other strong and dominating peaks identifying the buffer. The main Raman bands from Tris-HCl-based buffers are reported in Tables S1 and S2. As resumed in Table S2, the Tris-cation has been autonomously sieved from the DNA bundles, and its presence can be detected only in the dehydration residual. The same spectra are overlapped in Figure S1.

In samples with PBS (Phosphate-buffer saline), the main working buffer contributions at 538, 885, 980 and 1067 cm^{-1} are detected on buffer deposited on CaF2 slides and on the droplet residual, as in the other cases of study. PBS fingerprint was not dominant on suspended DNA and on DNA reference sample (on CaF_2 slide) as detailed in Table S3.

For solutions containing HEPES and $NiCl_2$, spectral features at 768, 797, 831, 889, 1039, 1068, 1143 and 1195 cm^{-1} were assigned to the buffer and the DNA when deposited on CaF_2 windows (see Table S4). The DNA fingerprint has been univocally assigned only in the range 1550–1700 cm^{-1} and related to the ring mode of dA and dG (1577 cm^{-1}) and the carbonyl stretch in thymine (1668 cm^{-1}; Figures 2c and 3d). The spectra of the pristine DNA molecules are severely affected by the buffer presence: the substantial contribution all over the range analyzed does not allow an unambiguous assignment to phosphodiester and bases vibrations. The Raman bands of the buffering agents overlap with several of the characteristic lines of the nucleic acids; furthermore, several structural markers are shifted with respect to the interfering lines, eventually broadening the peaks. In both cases, it is not possible to distinguish between the DNA fingerprint and the buffer contribution univocally.

The DNA samples suspended on SHS showed clearer spectra, allowing a straightforward peak assignment. Phosphate backbone vibration is centered at 787 cm^{-1}, and the overlap of the buffer signal observed for the sample deposited on CaF_2 has not been detected. A few lines of the suspended DNA showed the same Raman wavenumbers of the buffer bands. The 1:1 intensity ratio between the 768 and 831 cm^{-1} bands in the buffer is not present in the DNA spectra; we can assume the peak centered at around 832 cm^{-1} in the suspended DNA is related to the O-P-O stretch rather than a buffer contribution (Figure 4a).[34,38,39]

The band at 1045 cm^{-1} in the suspended DNA spectra is shifted compared to the buffer contribution, centered at approximately 1041 cm^{-1}, allowing the univocal assignment of the DNA phosphodiester CO stretching (Figure 4b). The peaks fitting in the range 1290–1350 showed two peaks with possible attribution to the buffer and the suspended DNA (1298 and 1327 cm^{-1}) (Figures 4c and S2). Anyway, the absence of the buffer contribution in the suspended DNA spectra allows

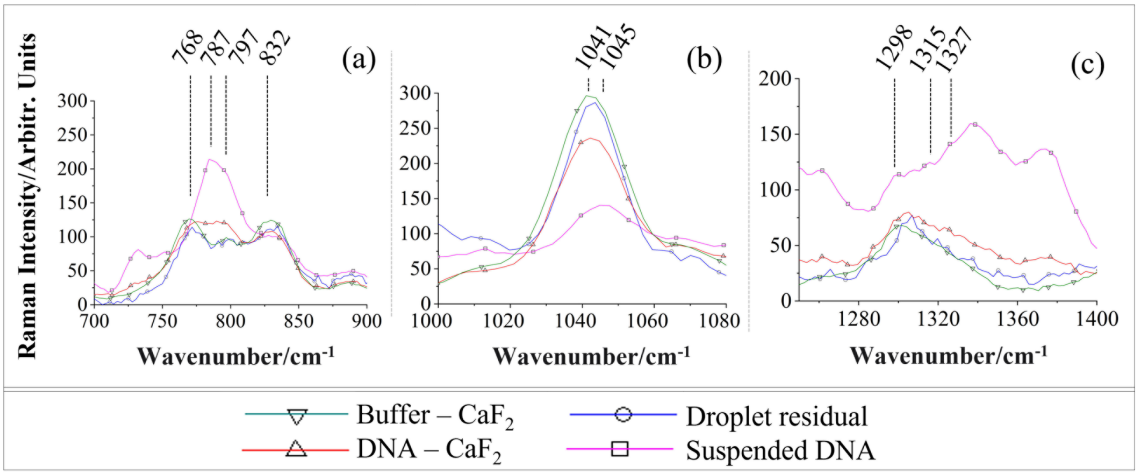

FIGURE 4 Details of the samples with $NiCl_2$ + HEPES buffer. Zoomed view of the areas where the spectra of the suspended DNA and of the working buffer solution overlap, more precisely in the ranges (a) 700–900 cm^{-1}, (b) 1000–1080 cm^{-1} and (c) 1270–1400 cm^{-1}. The wavenumber assignment is reported in each panel [Colour figure can be viewed at wileyonlinelibrary.com]

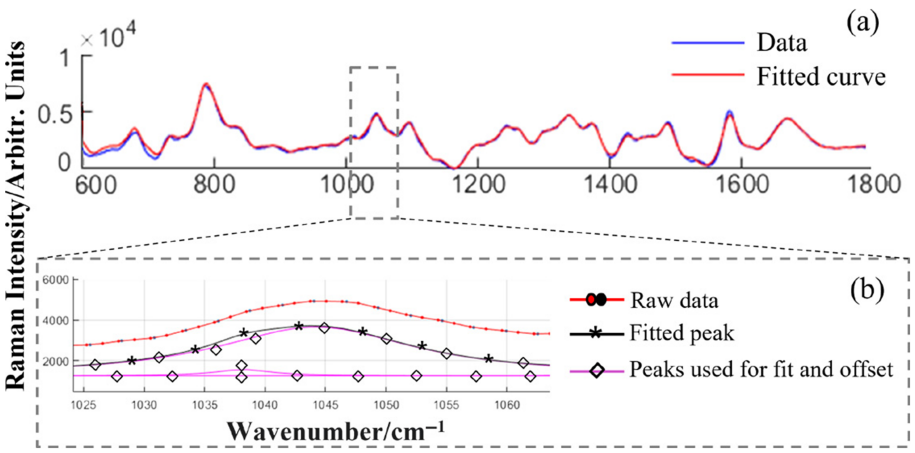

FIGURE 5 Example of fitted data. (a) Spectra fitted with 100 Lorentzian peaks and (b) inset representing the fit of one peak of interest at ~1045 cm^{-1}. The red line represents the raw data, while the black line the fitted peaks subtracted of the offset. In purple are shown the two peaks used for the fit and the offset (flat line) [Colour figure can be viewed at wileyonlinelibrary.com]

assigning the peaks undoubtedly to the DNA. Lines in the range 1400–1550 cm^{-1} and overlapping with buffer were assigned to DNA contribution due to differences in peaks shape and intensity ratios. Also, the prominent bands of the buffer can be assigned to the droplet residual (765, 795, 830, 890, 1041, 1065 and 1195 cm^{-1}) along with DNA-related peaks such as vibrations due to helix conformation (670 cm^{-1}), bases ring breathing (739, 1041, 1305 and 1470 cm^{-1}), phosphodiester backbone (790 cm^{-1}) and CH_2 bending (1445 cm^{-1}). Tentative assignment and buffer contributions are reported in Table S4.

As demonstrated by the SEM images and the Raman spectra acquired, the SHS approach has several and significative outcomes: (i) the concentration of not interacting molecules; (ii) their transport in specific areas of the device; (iii) the consequent separation of residual solution particles from the system under investigation effect; (iv) the ordering of self-assembly of DNA molecules by their suspension over micro-pillars; (v) the possibility to prepare optimal sieved molecules with no additional preparation steps for the analysis and (vi) the possibility to measure self-assembly of DNA without drawbacks of more conventional techniques.

We want to remark that the spectra acquired in different points along the suspended DNA and on several suspended bundles did not show any overlap with the buffering agents; on the other side, the same nucleic acid sample deposited on a CaF_2 surface showed such high contributions from the solution that prevented the clear assignation of Raman peaks. Molecules such as HEPES were not detected in the bundle but were only located in the droplet residual in which the non-interacted molecules are concentrated. A similar evaluation applies to all the buffers used in this work.

3 | CONCLUSIONS

Albeit the buffer contribution affects the DNA spectra when evaluated on CaF_2 windows, we found that DNA spectra acquired on suspended filaments did not show a buffer-related signature. As expected, the buffer interference is detected again while studying the droplet residual, suggesting that the optimized SHS can separate small non-interacted molecules from the suspended filaments. Equally important is that SHS devices concentrate non-interacted material in the final point of the droplet evaporation. All the evidence suggests that the helices retain only ions efficiently interacted with DNA and the compounds in excess or non-interacted are sieved away from the areas of interest. The self-sieving effect occurring on SHS allowed the self-cleaning of the helices and the concentration of the interfering molecules in a limited area of the device far from the acquisition area. With this approach, the genetic material used did not need any additional preparative purification from the interfering buffering agents and the non-interacted molecules excesses.

The proposed approach has the tremendous experimental advantage to offer to the spectral investigation a readily identifiable sample's area: suspended specimen strands in a background-free environment, confined and spatially oriented along the pillars direction. Directly accessible representative essays of biomaterial obtained with SHS technique without needing a preliminary reduction into fibers overcomes one of the main limitations of traditional X-Ray crystallography. The use of pristine DNA and its interactions with different buffers have to be considered a starting point to validate the reproducibility of the results. This strategy will be applied to the interactions between DNA and molecules with a strong influence on nucleic acids conformation and

function such as chemotherapy agents or heavy metals. This will provide complete information on structural and morphological details of biomolecules and their relation with the surrounding environment, providing an alternative approach for biomedical, biochemical and biophysical purposes.

4 | EXPERIMENTAL

4.1 | Superhydrophobic devices fabrication

As previously reported in Marini et al.,[12,15] the devices used are superhydrophobic surfaces with silicon (Si <100>) micro-fabricated pillars, characterized by a height of 10 μm, diameter of 6 μm and a pillar-pillar inter distance (edge to edge) of 12 μm. The pattern of pillars is defined by a combination of positive optical lithography and sputtered metal deposition (10 nm of Ti, 50 nm of Au and 50 nm of Cr), followed by lift-off. The device is DRIE etched to define the micro-structures height and the Cr protective layer removed by wet etching. The subsequent functionalization of the device with a monolayer of perfluoro-decyl trichlorosilane (FDTS) guarantees the final super-hydrophobicity of the system.

4.2 | Solutions preparation

The DNA of lambda phage has been used due to its length, the commercial availability and the reproducibility of the sequence and purchased from New England Biolabs (NEB). An aliquot of the DNA stock solution was diluted in different saline buffers to reach a final concentration of 50 ng/μl. The following buffers have been used:

1. Phosphate-buffer saline 1X (PBS, 1.37 mM NaCl, 27 mM KCl, 100 mM Na_2HPO_4, 18 mM KH_2PO_4).
2. 6.5 mM NaCl and 10 mM Tris-HCl, pH 9.3.
3. 1.5 mM $MgCl_2$, 10 mM Tris-HCl pH 7.4.
4. 20 mM $NiCl_2$, 10 mM HEPES pH 7.0.

The buffers were filtered using a 0.2 μm syringe filter (Millipore, Billerica, MA, USA) and stored at room temperature. Each freshly prepared DNA/buffer solution was warmed in a thermocycler (BioRad, US) at 65°C for 10 min and then kept at 37°C prior to use. The silicon device was pre-heated and maintained on a hot plate to ensure a controlled temperature of 25°C. A droplet of 5 μl volume was pipetted on the superhydrophobic device and kept at 63% RH until the complete evaporation of the buffer solution. The negative control λDNA solution and the buffer used were separately drop casted on CaF_2 windows (Crystran Ltd., Dorset, UK) and were characterized after dehydration.

4.3 | Characterization of the DNA samples

4.3.1 | Scanning Electron Microscopy

The results of the deposition process were imaged using a Quanta 200 SEM (ThermoFisher Scientific, Oregon, USA) working at a beam energy of 3 kV and a current of 43 pA. Additional preliminary treatments such as coating were not performed on the samples, to avoid any additional contribution to the bundle composition analyzed by Raman spectroscopy.

4.3.2 | Raman spectroscopy

We characterized samples using a WITec confocal Raman system (α-Raman WITec GmbH, Ulm, Germany), equipped with a 100X Zeiss objective, NA = 0.9 and a dispersive grating of 600 gr/mm that images a 100 μm core fiber, used to couple microscope to the $f = 320$ mm spectrometer, as the input slit aperture on a 1×2048 pixels CCD (Newtown CCD, Andor, −80°C thermoelectric cooled). A solid-state laser, 532 nm, power of 1.9 mW, was used as the excitation line. Each measure was obtained accumulating 60 spectra, each with an exposure time of 1 s. Several tens of measures of different areas of the SHS (droplet residual and bundles) and of the dehydrated drops on CaF_2 were acquired using the Control Four/Five (WiTec) software.

The Raman wavenumber of the spectra was calibrated by means of a Lorentzian fit on a reference peak (521 cm^{-1} for the SHS or 321 cm^{-1} for CaF_2). A 6th order polynomial background subtraction method based on the algorithm proposed by Lieber and Mahadevan-Jansen[40] was used (Figure 5). The algorithm was typically applied in the spectral region 200–2000 cm^{-1} to exclude from the correction method information not related to the aim of this paper such as the main water Gaussian peaks in the region 2900–3800 cm^{-1}. The spectral contribution of each peak was evaluated by fitting a set of Lorentzian curves in the background-subtracted data. Initial fitting parameters were evaluated starting from a comb of peaks and recursively refining the parameters starting from previous iteration results, excluding peaks with amplitude comparable with the noise level and with full width at half maximum (FWHM) < 2 cm^{-1} and larger then typically 100 cm^{-1}, that is, not corresponding to a single peak. Larger bands were fitted as a group of overlapping peaks.

In all the cases, the number of peaks to be used has been chosen to maximize the adjusted R^2 parameter at each fit. Background removal and fit procedure was implemented in MATLAB environment. For the sieving analysis, spectra of the Tris-based samples were normalized in the range 1455–1470 cm^{-1}, in the range 950–100 cm^{-1} for the PBS-based samples and to the 1041 cm^{-1} peak for the $NiCl_2$ based.[33,34,39]

ACKNOWLEDGEMENT

This research did not receive any specific grant from funding agencies in the public, commercial or not-for-profit sectors. Open Access Funding provided by Politecnico di Torino within the CRUI-CARE Agreement. Correction added on July 02, 2022, after first online publication: CRUI funding statement has been added.

CONFLICT OF INTEREST

The authors declare no competing interest.

DATA AVAILABILITY STATEMENT

The data that support the findings of this study are available from the corresponding author upon reasonable request.

ORCID

Monica Marini https://orcid.org/0000-0001-8182-5239

REFERENCES

[1] L. Piantanida, D. Naumenko, E. Torelli, M. Marini, D. M. Bauer, L. Fruk, G. Firrao, M. Lazzarino, *Chem. Commun. Chem. Commun* **2015**, *51*, 4789.
[2] M. Xiao, W. Lai, T. Man, B. Chang, L. Li, A. R. Chandrasekaran, H. Pei, *Chem. Rev.* **2019**, *22*, 11631.
[3] E. Miele, A. Accardo, A. Falqui, M. Marini, A. Giugni, M. Leoncini, F. de Angelis, R. Krahne, E. D. E. D. Fabrizio, *Small* **2015**, *11*, 134.
[4] J. Doyle, *Molecular Techniques in Taxonomy*, Springer, Berlin, Heidelberg **1991**, 283.
[5] M. Tagliavia, A. Nicosia, F. Gianguzza, *Anal. Biochem.* **2009**, *385*, 182.
[6] R. Shi, R. S. Lewis, D. R. Panthee, *PLoS ONE* **2018**, *13*, e0203011.
[7] K.-H. Esser, W. H. Marx, T. Lisowsky, *Biotechniques* **2005**, *39*, 270.
[8] S. A. Thatcher, *Clin. Chem.* **2015**, *61*, 89.
[9] S. L. Beaucage, M. H. Caruthers, *Tetrahedron Lett.* **1981**, 22, 1859. https://doi.org/10.1016/S0040-4039(01)90461-7
[10] L.-F. Song, Z.-H. Deng, Z.-Y. Gong, L.-L. Li, B.-Z. Li, *Front. Bioeng. Biotechnol.* **2021**, *9*, 11631. https://doi.org/10.3389/fbioe.2021.689797
[11] P. Zhang, M. Moretti, M. Allione, Y. Tian, J. Ordonez-Loza, D. Altamura, C. Giannini, B. Torre, G. Das, E. Li, S. T. Thoroddsen, S. M. Sarathy, I. Autiero, A. Giugni, F. Gentile, N. Malara, M. Marini, E. di Fabrizio, *Commun. Biol.* **2020**, *3*, 457.
[12] M. Marini, T. Limongi, A. Falqui, A. Genovese, M. Allione, M. Moretti, S. Lopatin, L. Tirinato, G. Das, B. Torre, A. Giugni, F. Cesca, F. Benfenati, E. di Fabrizio, *Nanoscale* **2017**, *9*, 2768. https://doi.org/10.1039/C6NR07958J
[13] F. Gentile, M. Moretti, T. Limongi, A. Falqui, G. Bertoni, A. Scarpellini, S. Santoriello, L. Maragliano, R. Proietti Zaccaria, E. di Fabrizio, *Nano Lett.* **2012**, *12*, 6453.
[14] F. de Angelis, F. Gentile, F. Mecarini, G. Das, M. Moretti, P. Candeloro, M. L. Coluccio, G. Cojoc, A. Accardo, C. Liberale, R. P. Zaccaria, G. Perozziello, L. Tirinato, A. Toma, G. Cuda, R. Cingolani, E. di Fabrizio, *Nat. Photonics* **2011**, *5*, 682.
[15] M. Marini, A. Falqui, M. Moretti, T. Limongi, M. Allione, A. Genovese, S. Lopatin, L. Tirinato, G. Das, B. Torre, A. Giugni, F. Gentile, P. Candeloro, E. di Fabrizio, *Sci. Adv.* **2015**, *1*, e1500734.
[16] S. Stassi, M. Marini, M. Allione, S. Lopatin, D. Marson, E. Laurini, S. Pricl, C. F. Pirri, C. Ricciardi, E. di Fabrizio, *Nat. Commun.* **2019**, *10*, 1690.
[17] M. Marini, M. Allione, S. Lopatin, M. Moretti, A. Giugni, B. Torre, E. di Fabrizio, *Microelectron. Eng.* **2018**, *187–188*, 39.
[18] R. E. Franklin, R. G. Gosling, *Nature* **1953**, *171*, 740.
[19] G. Pezzotti, *J. Raman Spectrosc.* **2021**, *52*, 2348.
[20] M. Moretti, M. Allione, M. Marini, B. Torre, A. Giugni, T. Limongi, G. Das, E. di Fabrizio, *Microelectron. Eng.* **2017**, *178*, 194.
[21] M. Marini, G. Das, R. la Rocca, F. Gentile, T. Limongi, S. Santoriello, A. Scarpellini, E. di Fabrizio, *Microelectron. Eng.* **2014**, *119*, 151.
[22] M. Marini, M. Allione, B. Torre, M. Moretti, T. Limongi, L. Tirinato, A. Giugni, G. Das, E. di Fabrizio, *Microelectron. Eng.* **2017**, *175*, 38.
[23] J. Shi, C. Zhu, Q. Li, Y. Li, L. Chen, B. Yang, J. Xu, Y. Dong, C. Mao, D. Liu, *Macromol. Rapid Commun.* **2021**, 42, 2100182.
[24] M. Marini, T. Limongi, M. Moretti, L. Tirinato, E. di Fabrizio, *La Riv. del Nuovo Cim.* **2017**, *40*, 241.
[25] F. Gentile, M. L. Coluccio, N. Coppede, F. Mecarini, G. Das, C. Liberale, L. Tirinato, M. Leoncini, G. Perozziello, P. Candeloro, F. de Angelis, E. di Fabrizio, *ACS Appl. Mater. Interfaces* **2012**, *4*, 3213.
[26] J. M. Benevides, G. J. Thomas, *Nucleic Acids Res.* **1983**, *11*, 5747.
[27] J. M. Benevides, P. L. Stow, L. L. Ilag, N. L. Incardona, G. J. Thomas, *Biochemistry* **1991**, *30*, 4855.
[28] G. J. Thomas, P. Serwer, *J. Raman Spectrosc.* **1990**, *21*, 569.
[29] D. Serban, J. M. Benevides, G. J. Thomas, *Biochemistry* **2002**, 41, 847. https://doi.org/10.1021/bi011004z
[30] G. J. J. Thomas, J. M. M. Benevides, S. A. A. Overman, T. Ueda, K. Ushizawa, M. Saitoh, M. Tsuboi, *Biophys. J.* **1995**, *68*, 1073.
[31] G. J. Thomas, A. H.-J. Wang, *Nucleic acids Mol. Biol.* **1988**, *2*, 1.
[32] B. Prescott, W. Steinmetz, G. J. Thomas, *Biopolymers* **1984**, *23*, 235.
[33] J. Duguid, V. A. Bloomfield, J. Benevides, G. J. Thomas, *Biophys. J.* **1993**, *65*, 1916.
[34] J. G. G. Duguid, V. A. Bloomfield, J. M. M. Benevides, G. J. J. Thomas, *Biophys. J.* **1995**, *69*, 2623.

[35] R. C. Lord, G. J. Thomas, *Spectrochim. Acta Part A Mol. Spectrosc.* **1967**, *23*, 2551.
[36] S. Ponkumar, P. Duraisamy, N. Iyandurai, *Am. J. Biochem. Biotechnol.* **2011**, *7*, 135.
[37] N. Leulliot, V. Baumruk, M. Abdelkafi, P. Y. Turpin, A. Namane, C. Gouyette, T. Huynh-Dinh, M. Ghomi, *Nucleic Acids Res.* **1999**, *27*, 1398.
[38] L. Movileanu, J. M. Benevides, G. J. Thomas, *J. Raman Spectrosc.* **1999**, *30*, 637.
[39] J. G. Duguid, V. A. Bloomfield, J. M. Benevides, G. J. Thomas, *Biophys. J.* **1996**, *71*, 3350.
[40] C. A. Lieber, A. Mahadevan-Jansen, *Appl. Spectrosc.* **2003**, *57*, 1363.

SUPPORTING INFORMATION

Additional supporting information may be found in the online version of the article at the publisher's website.

How to cite this article: M. Marini, B. Torre, M. Allione, T. Limongi, F. Legittimo, A. Giugni, C. Ricciardi, C. F. Pirri, E. di Fabrizio, *J Raman Spectrosc* **2022**, *53*(8), 1352. https://doi.org/10.1002/jrs.6368